Geophysical Research Letters®

Key Points:

- Ions in an observed jet exhibit complex distribution functions, with a cold/fast jet beam and hotter/slower background population
- Jet interaction with the background magnetosheath is studied by comparing partial moments of the jet population with the full ion moments
- The derived properties of the cold/fast population connect the jet's origin to upstream solar wind and foreshock structures

Supporting Information:

Supporting Information may be found in the online version of this article.

Correspondence to:

S. Raptis,
savvra@kth.se;
savvasraptis@gmail.com

Author Contributions:

Conceptualization: Savvas Raptis
Data curation: Savvas Raptis
Formal analysis: Savvas Raptis
Funding acquisition: Tomas Karlsson
Investigation: Savvas Raptis
Methodology: Savvas Raptis
Project Administration: Savvas Raptis
Software: Savvas Raptis
Supervision: Tomas Karlsson, Andris Vaivads
Validation: Savvas Raptis
Visualization: Savvas Raptis
Writing – original draft: Savvas Raptis

On Magnetosheath Jet Kinetic Structure and Plasma Properties

Savvas Raptis[1] ![ORCID], **Tomas Karlsson**[1] ![ORCID], **Andris Vaivads**[1] ![ORCID], **Martin Lindberg**[1] ![ORCID], **Andreas Johlander**[2], and **Henriette Trollvik**[1] ![ORCID]

[1]Division of Space and Plasma Physics, KTH Royal Institute of Technology, Stockholm, Sweden, [2]Swedish Institute of Space Physics, Uppsala, Sweden

Abstract High-speed plasma jets downstream of Earth's bow shock are high velocity streams associated with a variety of shock and magnetospheric phenomena. In this work, using the Magnetosphere Multiscale mission, we study the properties of a jet found downstream of the Quasi-parallel bow shock using high-resolution (burst) data. By doing so, we demonstrate how the jet is an inherently kinetic structure described by highly variable velocity distributions. The observed distributions show the presence of two plasma population, a cold/fast jet and a hotter/slower background population. We derive partial moments for the jet population to isolate its properties. The resulting partial moments appear different from the full ones which are typically used in similar studies. These discrepancies show how jets are more similar to upstream solar wind beams compared to what was previously believed. Finally, we explore the consequences of our results and methodology regarding the characterization, origin, and evolution of jets.

Plain Language Summary Typically, particles from the Sun get strongly decelerated when they interact with the magnetic field of Earth, forming a shock wave. Magnetosheath (MSH) jets are fast streams of particles appearing downstream of this shock, with typically higher velocities and densities than the background population. In this work, we show how jets behave after they are created at the shock wave. We describe the variability of their properties and how this is connected to the background MSH population they interact with. Through that, we reveal new insights regarding their origin, evolution, and motivate on a new approach to study jets and similar phenomena in the future.

1. Introduction

As the supersonic solar wind (SW) approaches Earth, it interacts with the planet's magnetic field, forming a bow shock. Downstream of the shock, the magnetosheath (MSH) region forms, which is a highly turbulent plasma environment where several phenomena co-exist. One of these phenomena is the so called MSH jets and during the last two decades, they have drawn considerable attention (Plaschke et al., 2018). These jets are transient dynamic pressure enhancement with respect to the downstream ambient background plasma. The dynamic pressure enhancements can be due to either a velocity and/or density increase (Archer et al., 2012).

One of the most important features that determines the properties of jets is whether they are found in the so called Quasi-parallel (Qpar) or Quasi-perpendicular (Qperp) MSH. These regions are, respectively, the plasma downstream of a Qpar or a Qperp shock crossing. Typically, the distinction between Qpar and Qperp shock crossings is based on the angle between the upstream Interplanetary Magnetic Field vector and the bow shock normal vector. If the angle is less than 45°, we call the crossing Qpar, while if it is greater, we call it Qperp. The downstream MSH of the Qpar shocks is more turbulent, exhibits lower temperature anisotropy, and contains more high-energy particles (Fuselier, 1994; Karlsson et al., 2021; Raptis, Karlsson, et al., 2020). The complexity of Qpar shocks also extends upstream of the shock to the foreshock region where non-linear ULF waves, field-aligned beams and wave-particle interaction regions are observed (Battarbee et al., 2020; Eastwood et al., 2005; Wilson, 2016). It has been shown that jets appear more frequently behind the Qpar shock rather than the Qperp one (Raptis, Aminalragia-Giamini, et al., 2020; Raptis, Karlsson, et al., 2020; Vuorinen et al., 2019), and typically have significant effects on the geomagnetic environment of Earth (Plaschke et al., 2018). For example, they can enhance or initiate magnetopause reconnection (Escoubet et al., 2020; Hietala et al., 2018; Ng et al., 2021; Vuorinen et al., 2021), accelerate particles (Liu et al., 2019, 2020), generate a variety of different waves in the MSH and

outer magnetosphere environment (Archer et al., 2019, 2021; Katsavrias et al., 2021) and even have effects on the inner magnetosphere and ionosphere (Hietala et al., 2012; Norenius et al., 2021; Wang et al., 2018).

The origin of MSH jets is still under debate. Regarding jets found downstream of a Qperp shock, they have been associated with a variety of different phenomena such as reconnection exhausts, mirror mode waves and magnetic flux tubes (Blanco-Cano et al., 2020; Kajdič et al., 2021). Downstream of the Qpar shock, jets have been associated with several other generation mechanisms, from shock ripples (Hietala et al., 2009; Hietala & Plaschke, 2013) to upstream rotational discontinuities (Archer et al., 2012; Dmitriev & Suvorova, 2012) and reconnection (Preisser et al., 2020). More recently, investigations have focused on the connection of jets to upstream foreshock structures (Karlsson et al., 2015; Omelchenko et al., 2021; Sibeck et al., 2021; Suni et al., 2021) and to the reformation of the Qpar shock (Raptis et al., 2022). While the exact generation mechanism of these structures is still under investigation, the connection to SW properties such as the cone angle and transient events has been demonstrated in various recent studies, indicating that there is a direct link between SW conditions and MSH jets (Koller et al., 2022; LaMoury et al., 2021; Plaschke et al., 2013; Tinoco-Arenas et al., 2022).

Overall, jets have been studied extensively, and have been connected to various phenomena. Furthermore, most of the research is typically done through the use of full particle moments, assuming that these accurately represent jet properties. However, in other phenomena of similar nature (transient and localized), such as reconnection jets, it has been shown that this is not necessarily the case (Goldman et al., 2020). In magnetic reconnection, a colder jet is measured along with a hotter and slower background plasma (Y.-X. Li et al., 2021). Moreover, it was shown recently that by investigating the partial moment of jets, their properties resemble more the undisturbed SW properties (Raptis et al., 2022).

In this work, using the Magnetosphere Multiscale (MMS) mission, we will first address if the underlying assumption that full plasma moments can accurately describe the jet population is valid. To achieve this, we examine a typical jet found in the turbulent Qpar MSH. We show how the jet properties vary throughout its interaction with the background plasma. We then proceed with separating the background and the jet population and derive the jet's partial plasma moments. The jet will be the colder and faster part of the velocity distribution function (VDF) while the background the more thermalized and slowed down part. Then, we present the resulting discrepancies between the partial and full ("raw") plasma moments. A discussion follows, focusing on the implications of the results on the jet characterization and evolution. Finally, we comment on the results shown in previous studies, while proposing a series of future extensions.

2. Method

For the analysis, we use two different coordinate systems. The Geocentric Solar Ecliptic (GSE), and a field-aligned coordinate system. For the field-aligned system, we define x to be parallel to the locally measured magnetic field $\mathbf{B}$, y to be along $\mathbf{v} \times \mathbf{B}$, with $\mathbf{v}$ being the ion velocity, and finally z completes the coordinate system.

2.1. Data

Due to the small separation of the tetrahedron formation between the MMS satellites, we primarily use data from MMS1. The rest of the satellites (MMS2-4) show, as expected, very similar observations (panels b–d of Figure 1). For the magnetic field measurements, we use the fluxgate magnetometer (Russell et al., 2016) which has a resolution of 0.0625 s in the survey mode that was used. For the ion measurements (moments and distribution functions) we use the fast plasma investigation (FPI; Pollock et al., 2016) which has a time resolution of 4.5 s in fast mode and 0.15 s in burst mode. Finally, for the comparison with the upstream SW measurements and for the bow shock and magnetopause location modeling we use the OMNIWeb database (King & Papitashvili, 2005).

2.2. Jet Moment Derivation

As discussed below in the results section, the jet population exhibits properties indicating that the full ("raw") plasma moments may not accurately describe the jet population, but rather two populations combined, the jet and the background MSH. Therefore, we will use two different ways to derive partial ion moments to isolate the jet population. The first approach is to remove the parts of the VDF corresponding to significantly different velocities from the plasma flow, as described by the full moments. This is done by removing measurements that are
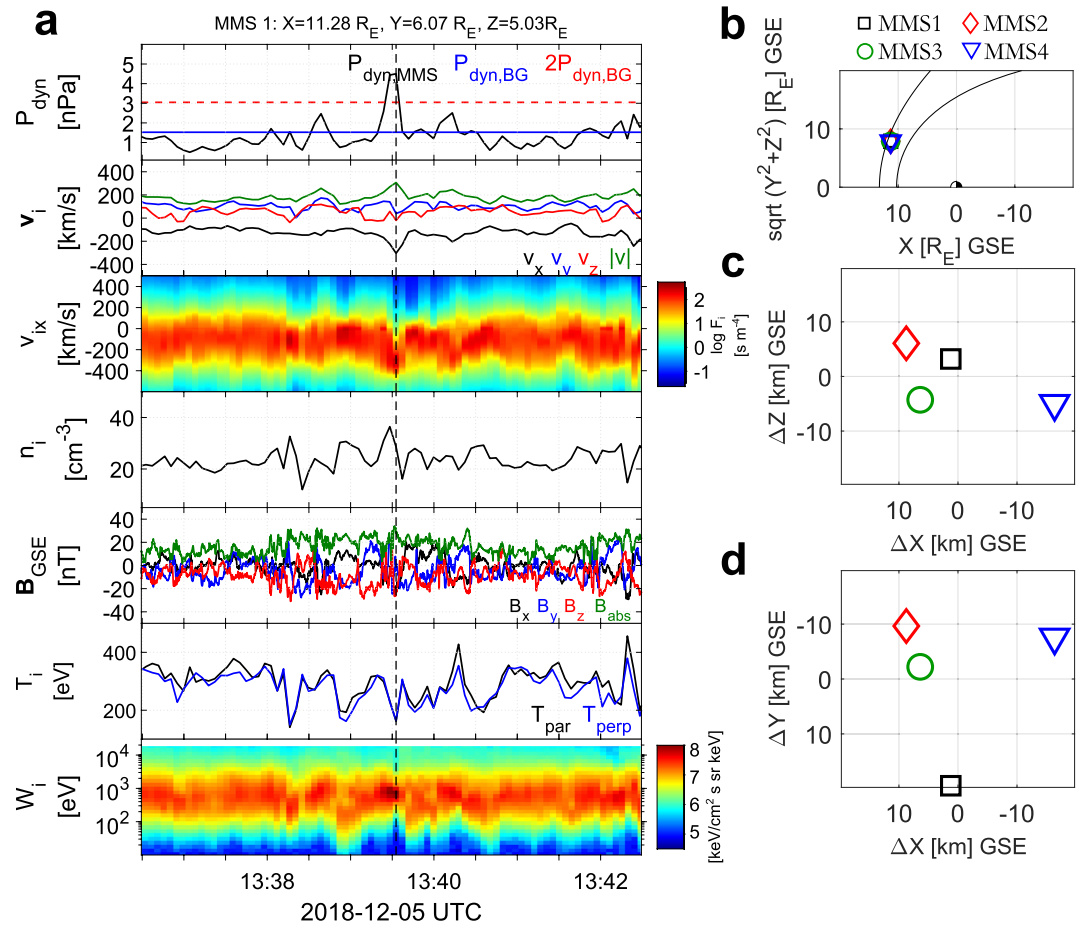
Figure 1. (a) Fast mode particle and survey field measurements of MMS1 corresponding to ±3 min from the dynamic pressure peak (at 13:39:32), corresponding to a magnetosheath (MSH) jet. (Top–bottom) Ion dynamic pressure $(m_p n_i V_i^2)$, along with background MSH levels $P_{dyn,BG}$, ion velocity in Geocentric Solar Ecliptic (GSE) coordinates, reduced 1D ion velocity distribution function in the x GSE direction, ion number density, magnetic field measurements, ion temperature in parallel and perpendicular to **B** directions, and ion differential energy spectrum. (b) Position of the Magnetosphere Multiscale (MMS) satellites with respect to Earth in GSE coordinates. Approximate positions of the bow shock and the magnetopause using upstream OMNIweb measurements and a model are plotted (Shue et al., 1998). Spacecraft separation in the (c) zx plane and (d) yx plane in GSE coordinates.

outside a sphere of radius equal to the thermal velocity (Vth) from the full VDF, centered around the ion velocity. Then we proceed with computing the ion moments from the remaining VDF. This method, is referred to as "cut" in the sections below. The second approach is to fit a function to the VDFs by assuming that a specific form is describing the observations. This method is refereed to as "fit." Both methods have strengths and weaknesses for the task we undertake. Finally, we also try to do the "fit" method after the "cut" method, for validating purposes. This produced essentially the same results as directly performing a fit, as we will see below.

The "cut" method is easy to implement and provides moments that in principle should characterize the jet population more accurately compared to the "raw" plasma moments. However, as we discuss below, this method typically fails to fully remove the background population since the thermal velocity is typically quite large in the MSH region and even when two populations co-exist they correspond to measurements closer than one Vth to each other in velocity space. It should be noted that this technique could work well when applied to foreshock events, since in that case, the reflected particles and the SW-beam like population are well separated from each other (e.g., Liu et al., 2017, 2022).

Regarding the fitting approach, we primarily focus on the properties derived by fitting a double (sum of two) Maxwellian on reduced (integrated) 1D VDFs. While MSH VDFs are typically close to Maxwellian (Safrankova et al., 1994), deviations are frequently observed (e.g., Graham et al., 2021; Perri et al., 2020). Similarly, the choice

of a Maxwellian, rather than a bi-Maxwellian, effectively means we assume a single temperature characterization for the plasma population, which again is not always the case (Lucek et al., 2005). However, these assumptions do not have a significant effect since we are using reduced 1D VDFs rather than the whole measured 3D VDF. Furthermore, there is no significant effect in the properties that we want to evaluate, these being primarily the ion velocity and density. The choice of the 1D VDFs was made in order to make the fitting process easy to implement for a time series analysis. We use the full moments given by the FPI measurements as initial values, while the small number of free parameters (1D) ensures a fast and valid convergence of the non-linear least squares fitting method. Finally, the majority of the discussion about jets has been done based on their earthward oriented velocity that is typically observed (see e.g., Archer & Horbury, 2013; Karlsson et al., 2015; Plaschke et al., 2018). We therefore focus primarily on the reduced 1D VDFs in the x GSE direction.

After two Maxwellians are fitted to the 1D VDFs, we obtain the moments based on the velocity (higher absolute velocity) and temperature (colder beam) that correspond to the jet population. To distinguish the jet population, we choose the distribution with the highest absolute velocity in the x GSE direction. For the y and z direction, we pick the coldest (beam-like) population via the estimation of the temperature. Since the fitting was done on the 1D reduced VDFs, the total temperature is defined as the average between each fit done on the 1D VDFs in GSE coordinates (($T_x + T_y + T_z$)/3). This was done to allow a direct comparison to the temperature of the full moments.

To validate our results, we examined the fitting process at a set of different times, using 3D VDFs, 2D and 1D reduced VDFs with various coordinate systems. This resulted in similar results for all methods. Variations based on the number of dimensions and coordinate system are on the order of ~5% for density. The temperature is harder to validate, since it changes depending on the coordinate system we use. However, comparing that temperature with the one derived using a field-aligned coordinate system produced similar results to the GSE. It should be noted that for the qualitative purpose of this work, these variations are reasonably low and have no effect on our conclusions. However, for completeness, we include in Figure S2 in Supporting Information S1 the 95% confidence intervals from the fitting procedure on the introduced plasma moments.

An overview plot of the downstream Qpar MSH and jet basic properties (using fast mode data) along with the MMS position and formation are shown in Figure 1. At approximately 13:39:30, by using the full particle moments, the jet fulfills the typical criterion of $P_{dyn} > 2P_{dyn,BG}$ used in similar works (e.g., Raptis, Karlsson, et al., 2020) as demonstrated in the first panel of Figure 1a. During the jet, the full moments from MMS show a maximum dynamic pressure of 4.5 nPa, while the maximum observed velocity is over 300 km/s and the density ~35 cm^{-3}. These properties correspond to a typical jet found downstream of the Qpar shock (Raptis, Karlsson, et al., 2020).

3. Results

Figure 2 shows high-resolution (burst) measurements of the jet shown in Figure 1, along with associated pre and post jet periods. In panel (a) we show several time series similar to Figure 1 and, in panels (b–e), the 2D reduced VDFs in two different coordinate systems for t_1 and t_2. We focus on two periods of the jet, the initial phase of the jet (t_1) and its end (t_2). These times respectively represent the peak of dynamic pressure (7.5 nPa) during the jet interval and the peak of absolute velocity (340 km/s).

Before we address the exact details of the jet, it is important to note the interaction of the jet with an observed magnetic structure. At approximately 13:39:28, there is a discontinuity in the magnetic field, resulting in a rotation of **B** as shown by the change in B_z and B_y. This rotation is associated with a magnetic structure of possibly bow shock or turbulent Qpar MSH origin. We can see this having a clear effect on the VDFs of the jet, observed both in the 2D reduced VDF (Figure 2b) and in the plasma moments, where a change in the direction of the velocity is clearly observed. Specifically, a variation in V_z and V_x takes place, following the presence of the discontinuity, indicating its effect on the plasma population. The speed of the discontinuity was estimated by using a timing method (see more information in chapters 12 and 13 of Paschmann and Daly (1998)). The normal vector was estimated as **n** = [−0.84, 0.49, 0.24]. For the estimation, we used the B_x component which has a similar variation in all spacecraft. The velocity was computed to be ~215 ± 30 km/s with respect to the spacecraft, where the error is estimated as the root mean square error (see e.g., Vogt et al., 2011). This makes the discontinuity slightly slower compared to the jet observations, for which the "raw" moments of the FPI along the normal vector of the discontinuity indicate an average speed of ~275 ± 10 km/s at the same time. The error of the velocity in
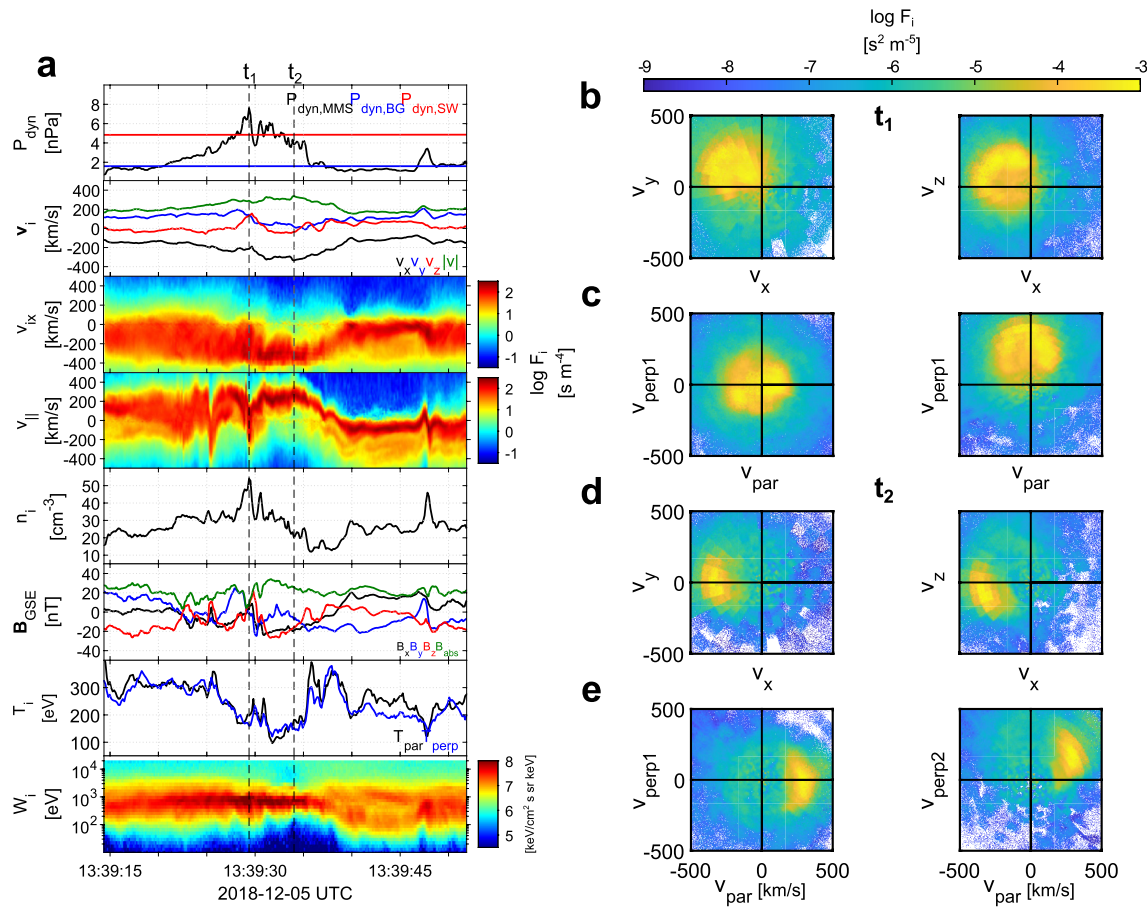
Figure 2. (a) Burst mode particle and survey field measurements of MMS1 corresponding to the jet observation. (Top–bottom) Ion dynamic pressure, along with background magnetosheath and solar wind levels, ion velocity in Geocentric Solar Ecliptic (GSE) coordinates, reduced 1D ion velocity distribution functions (VDFs) in the x GSE direction and parallel to the magnetic field, ion number density, magnetic field measurements, ion temperature in parallel and perpendicular to **B** directions, and ion differential energy spectrum. The two vertical dotted black lines represent the peak of dynamic pressure (t_1) and absolute velocity (t_2). (b) 2D reduced VDFs in GSE coordinates for t_1 in km/s, (c) 2D reduced VDFs in field-aligned coordinates for t_1 in km/s, (d) 2D reduced VDFs in GSE for t_2, and (e) 2D reduced VDFs in field-aligned coordinates for t_2 in km/s.

this case is computed as the average standard deviation of 10 projected velocity measurements before and after t_1. This essentially shows that the jet population that we discuss below likely has a higher velocity than the magnetic structure, along its normal, allowing an interaction to take place. This can be connected to general observations made, showing how a jet interacts with the background MSH, as discussed in previous works (Plaschke et al., 2017, 2020). Furthermore, at the end of the jet (13:39:40+) we see a change of sign of B_x, associated with a breaking of the Earthward and field-aligned flow.

If we compare Figures 1 and 2 we see how the burst data offer a more detailed and complex picture. Most noticeably, we see in the 1D reduced VDF how the jet (cold/fast part of the VDF) is primarily parallel to the magnetic field. It appears that during the jet observations, there are some striking differences in the distribution functions observed at t_1 compared to t_2. The first shows a much more thermalized population with a higher temperature and density, corresponding to the existence of a hot/slow MSH population co-existing with a colder/faster one. On the other hand, t_2 shows mainly a cold/fast SW-like plasma with primarily earthward velocity and limited thermalization and compression. These differences are shown both in the 1D VDFs and ion energy spectrum where we see how gradually going from t_1 to t_2, the beam-like structure of the jet is becoming more prominent. Furthermore, at the 2D VDFs of t_1 (panels b and c) one can see the same thermalized distribution, while for t_2 the primarily earthward (and field-aligned) beam corresponding to the jet is easily distinguishable.

We proceed with the application of the two different methods described above (cut and fit), to derive the partial plasma moments corresponding to the jet. The results are visualized in Figure 3. The cut method seems to provide
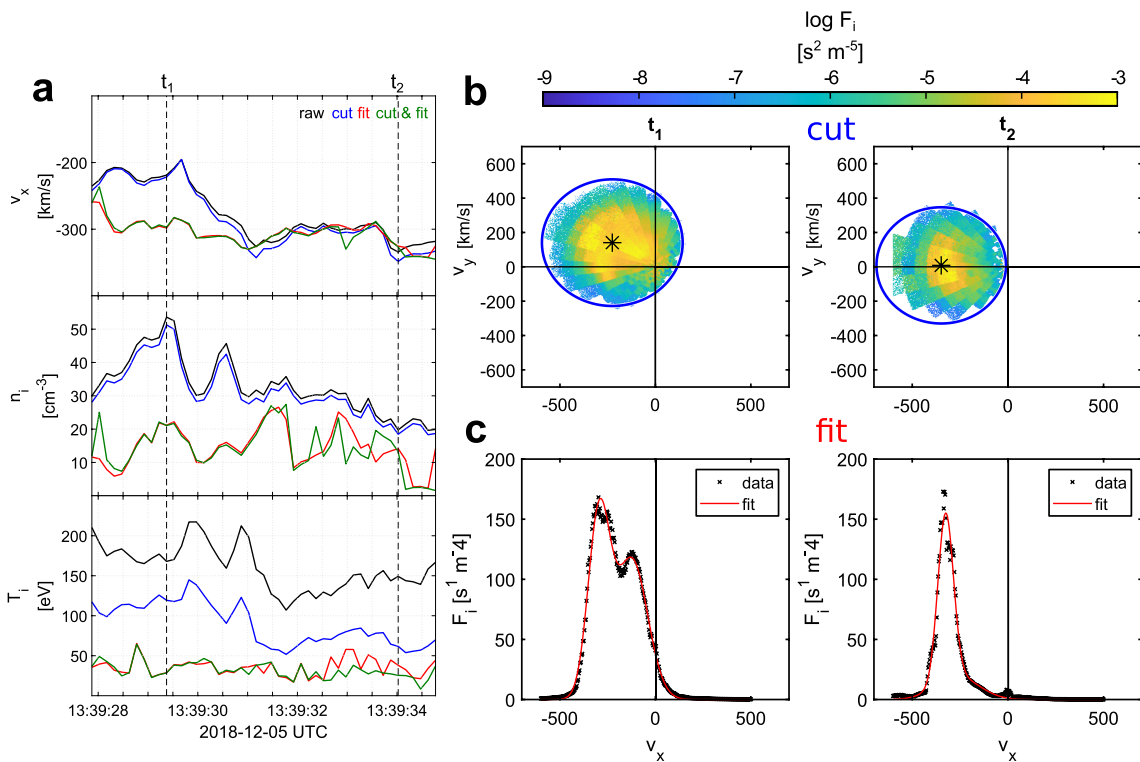
Figure 3. (a) (Top–bottom) Ion velocity in the x Geocentric Solar Ecliptic (GSE) direction, ion number density and ion temperature from the original Magnetosphere Multiscale full moments and for the three different approaches (fit, cut, cut and fit) discussed in the methodology section. The 1D reduced velocity distribution functions (VDFs) that are fitted are smoothed by averaging over ± 1 measurement point. (b) 2D reduced VDFs in xy GSE coordinates for t_1 and t_2 with removed data corresponding to measurements with higher velocity than a sphere with a radius of Vth. (c) 1D reduced VDFs in x GSE coordinate for t_1 and t_2 fitted with the sum of two Maxwellian distributions. The "cut and fit" method produced 1D VDFs that were virtually identical to the ones shown in panel (c).

slightly higher earthward velocity and slightly lower density. Also, since it effectively removes the high velocity tails, it essentially reduces the temperature of the plasma to roughly half. Moving on to the fitting procedure, we now see a significantly higher absolute velocity from the very beginning of the jet and a much lower density and temperature. When comparing the full moments to the ones derived by the "fit" method, we see how the jet quantities from the fit method, remain more similar throughout its duration. As discussed before, in Figures 3b and 3c at t_1, the jet is an isolated plasma population, with an equally prominent background co-existing in the velocity space, drifting with a lower $|V_x|$. This explains the large discrepancies that we observe between the fit and the cut moments shown in panel (a). On the other hand, at t_2, the background is strongly depleted. This results in very similar plasma moments between all methods, since effectively the plasma can be accurately described by a single population. For the error evaluation, in the supplementary information one can find the results of the "fit" method with their corresponding 95% confidence interval (Figure S1 in Supporting Information S1).

Below, we discuss these results and describe the implications they have to the jet characterization and evolution, while motivating the importance of adapting a similar kinetic-driven approach to future studies.

4. Discussion and Conclusions

We have shown a case study of a MSH jet observed downstream of the Qpar shock in a strongly turbulent MSH region. While a single event, it shows a series of new discovered properties and provides insight into Qpar jets. The most important results are summarized by the schematic and associated VDFs of Figure 4.

First, the jet appears to have a complex kinetic structure, with VDFs varying considerably throughout the observation. The variations of the VDFs appear to originate from the ongoing interaction with the MSH and its embedded magnetic structures.
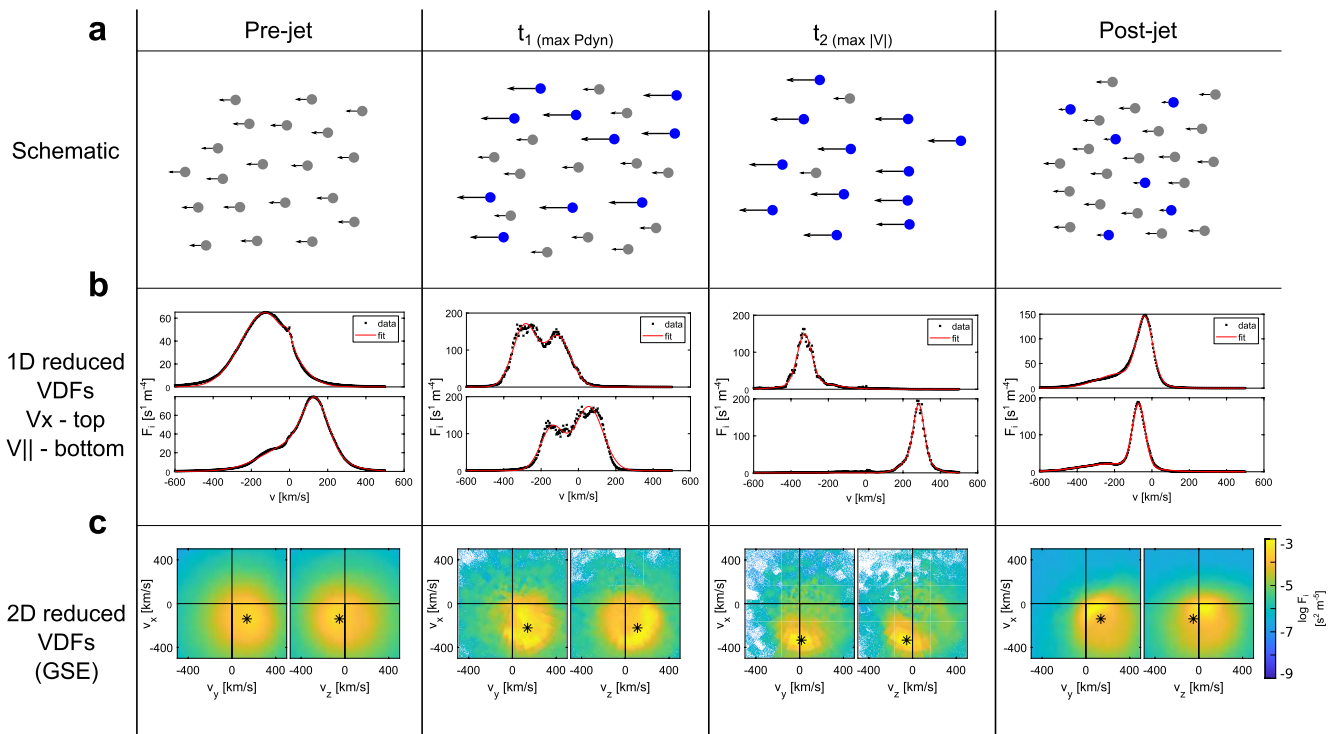
Figure 4. (Left–right) Pre-jet magnetosheath (MSH) corresponding to average distribution of 50 measurements during 13:39:14 to 13:39:21, t_1 corresponding to the peak of ion dynamic pressure, t_2 corresponding to the peak of absolute ion velocity, post-jet MSH corresponding to an average distribution of 40 measurements during 13:39:41 to 13:39:47. (a) Schematic of the interaction and the corresponding density/velocity profiles of the jet and background MSH population. Blue circles represent the jet population and gray the background MSH. (b) 1D reduced velocity distribution functions (VDFs) in x Geocentric Solar Ecliptic (GSE) coordinates and parallel to the magnetic field. (c) 2D reduced VDFs in GSE coordinates.

At this point, one of the most important conclusions we can draw is related to the origin of the high-speed jet. The origin of jets has been discussed much for several years, and many of the points made in previous studies were based on the properties of jets as shown directly through particle moments (see e.g., Raptis, Karlsson, et al., 2020). However, recently, as shown by simulations and observations (Raptis et al., 2022; Suni et al., 2021), jets appear to be directly connected to the foreshock dynamics for which a fluid approach and the particle moments may provide quite a limited picture (see e.g., Section 6.6 of Paschmann and Daly (1998)). Here, we show that if we consider the jet as an isolated population and perform a series of fits, it exhibits a SW-like profile. This profile consists of a SW-like velocity and a slightly enhanced density. Our results are therefore particularly consistent with the reformation generation mechanism and its associated observations (Raptis et al., 2022). The presented results are also consistent with the shock ripple mechanism (Hietala et al., 2009), but since there are no upstream measurements or indication of ripples, it is impossible to show any connection directly. It should be noted, though, that the presence of the discontinuity we briefly discussed, suggest a more complex formation mechanism. It has been previously discussed that other effects such as upstream foreshock waves and discontinuities may be related to jet formation (Raptis, Karlsson, et al., 2020). Recently, Omelchenko et al. (2021) showed how the formation and the penetration of jets into the MSH is directly connected to the turbulence-driven magnetic field variations, which is in agreement with the observations we present. Furthermore, such magnetic structures could locally deform the bow shock surface and then through a transfer mechanism (e.g., global reformation) allow both the SW and the embedded foreshock magnetic structures to get effectively transported downstream of Earth's bow shock. Finally, the lack of high energy ions at t_2, could possibly be explained by the discontinuity causing a local shock deformation which in turn changes the presence of downstream foreshock ions during the jet observation.

As shown in Figures 2 and 4, initially the background (Pre-jet) exhibits a Maxwellian like distribution with typical velocity and density profiles for the Qpar MSH. Then, the jet exhibits a strong interaction with the background (t_1) MSH and its magnetic field. The magnetic structure consisting of a discontinuity lies at its front, propagating toward the magnetosphere with a velocity lower than the jet population itself. Overall, the two populations

(background and jet) and their interaction result in a net increase in density and velocity, along with variations in the velocity direction. Later, we only see a clear SW-beam-like plasma population, similar to what was expected to occur in the MSH by Raptis et al. (2022). Generally, the jet propagates with its front edge consisting of a complex ongoing interaction region, while the rest of the jet (t_2) appears to be isolated with a depleted background. Eventually, if we look at the post-jet period (Figure 4), we see that a dense and stagnated population similar to the jet, residing in the velocity space along with the typical MSH background, possibly defining a previously unexplored end state of the jet phenomenon.

A further important implication of our results is that the isolated jet population may remain super-magnetosonic (with respect to the background MSH) when evaluating the partial moments, even if the full particle moments do not necessarily satisfy this condition. This could have implications regarding the generation of a secondary bow waves/shocks in the MSH and waves that can have an effect on electron acceleration, as recently discussed (Liu et al., 2020; Vuorinen et al., 2022). While this property is interesting, a more carefully analysis is required. Furthermore, the derived partial plasma moments of the jet showed that the ongoing interaction with the background could explain the different properties observed in jets close to the shock compared to jets close to the magnetopause. Recently, as shown by simulations, jets appear to have higher temperature and lower density and velocity as they evolve and propagate toward the magnetosphere (Palmroth et al., 2021). This could be explained by the ongoing interaction with the rest of the MSH and its magnetic field structures, as we demonstrated in this work.

The VDF profiles, observed at the initial stage of the jet (t_1), can be effectively modeled as two drifting Maxwellian distributions with different velocities. Such configurations can in principle drive a series of waves and explain previous observations made with respect to wave generation and variations in the magnetic field (Gunell et al., 2014; Karlsson et al., 2018; Katsavrias et al., 2021; Plaschke et al., 2017, 2020) in proximity to jets. Such wave generation and complex interaction that we demonstrate could also have an effect on the overall characterization of the MSH region regarding waves, current sheets and turbulence related phenomena typically observed (e.g., Gingell et al., 2021; H. Li et al., 2020; Vörös et al., 2019; Yordanova et al., 2020).

We want to conclude with an important point regarding the consequences of the methodology we used compared to what is usually implemented in statistical studies treating transient and localized phenomena such as MSH jets. Typically, most studies are built on the underlying assumption that full plasma moments can accurately describe the jet population. This is not the case, at least for a part of the jet, and it is still an open question how previous results that treat MSH jets in the turbulent Qpar MSH might be different if a similar approach to the one we present would have been applied. As discussed above, the jet properties estimated by our methods show a significantly lower density and higher absolute velocity, which results in a different total dynamic pressure profile. This opens the discussion regarding the validity of the definition that has been used so far (see discussion of Plaschke et al. (2018)). It is possible that the determination of not only the properties but of the existence of a jet would benefit by the direct use of the VDFs, especially in highly variable environments such as the Qpar MSH. Similar problems may arise due to different temporal resolution, as a comparison of Figures 1 and 2 shows.

It should be noted that there are several more jets that exhibit similar VDFs which we plan to study in the near future (we show two more examples in Supporting Information S1). The implication of plasma moment discrepancies along with further investigation of other jets and a comparison with simulation data is also already under investigation. Another interesting continuation would be to model and further analyze the post-jet period (Figure 4), which is beyond the scope of this letter. Furthermore, a natural continuation of this work would be to include more complex and accurate distribution models (3D bi-Maxwellians, kappa distributions, etc.) and perform more advanced fitting routines (e.g., considering fitting in log-space and using clustering techniques to determine the number of plasma populations). More importantly, non-Maxwellian distributions that we demonstrate in this work are the origin of wave generation and wave-particle interaction. Therefore, it is of great interest to determine what type of wave modes MSH jets can excite throughout their evolution as they interact with the background MSH and approach the magnetosphere. Finally, such complex interaction may have implications on the energy budget and the development of the jet (see e.g., Karlsson et al., 2018).

Data Availability Statement

References

Archer, M., Hartinger, M., Plaschke, F., Southwood, D., & Rastaetter, L. (2021). Magnetopause ripples going against the flow form azimuthally stationary surface waves. *Nature Communications*, *12*(1), 1–14. https://doi.org/10.1038/s41467-021-25923-7

Archer, M., Hietala, H., Hartinger, M. D., Plaschke, F., & Angelopoulos, V. (2019). Direct observations of a surface eigenmode of the dayside magnetopause. *Nature Communications*, *10*(1), 1–11. https://doi.org/10.1038/s41467-018-08134-5

Archer, M., & Horbury, T. (2013). Magnetosheath dynamic pressure enhancements: Occurrence and typical properties. In *Annales Geophysicae* (Vol. *31*, pp. 319–331).

Archer, M., Horbury, T., & Eastwood, J. (2012). Magnetosheath pressure pulses: Generation downstream of the bow shock from solar wind discontinuities. *Journal of Geophysical Research*, *117*(A5), A05228. https://doi.org/10.1029/2011ja017468

Battarbee, M., Blanco-Cano, X., Turc, L., Kajdič, P., Johlander, A., Tarvus, V., et al. (2020). Helium in the Earth's foreshock: A global Vlasiator survey. In *Annales Geophysicae* (Vol. *38*, pp. 1081–1099).

Blanco-Cano, X., Preisser, L., Kajdič, P., & Rojas-Castillo, D. (2020). Magnetosheath microstructure: Mirror mode waves and jets during southward IP magnetic field. *Journal of Geophysical Research: Space Physics*, *125*(9), e2020JA027940. https://doi.org/10.1029/2020ja027940

Dmitriev, A., & Suvorova, A. (2012). Traveling magnetopause distortion related to a large-scale magnetosheath plasma jet: THEMIS and ground-based observations. *Journal of Geophysical Research*, *117*(A8), A08217. https://doi.org/10.1029/2011ja016861

Eastwood, J., Lucek, E., Mazelle, C., Meziane, K., Narita, Y., Pickett, J., & Treumann, R. (2005). The foreshock. *Space Science Reviews*, *118*(1), 41–94. https://doi.org/10.1007/s11214-005-3824-3

Escoubet, C. P., Hwang, K.-J., Toledo-Redondo, S., Turc, L., Haaland, S., Aunai, N., et al. (2020). Cluster and MMS simultaneous observations of magnetosheath high speed jets and their impact on the magnetopause. *Frontiers in Astronomy and Space Sciences*, 78. https://doi.org/10.3389/fspas.2019.00078

Fuselier, S. A. (1994). Suprathermal ions upstream and downstream from the Earth's bow shock. *Washington DC American Geophysical Union Geophysical Monograph Series*, *81*, 107–119. https://doi.org/10.1029/GM081p0107

Gingell, I., Schwartz, S., Kucharek, H., Farrugia, C., & Trattner, K. (2021). Observing the prevalence of thin current sheets downstream of Earth's bow shock. *Physics of Plasmas*, *28*(10), 102902. https://doi.org/10.1063/5.0062520

Goldman, M., Newman, D., Eastwood, J., & Lapenta, G. (2020). Multibeam energy moments of multibeam particle velocity distributions. *Journal of Geophysical Research: Space Physics*, *125*(12), e2020JA028340. https://doi.org/10.1029/2020ja028340

Graham, D. B., Khotyaintsev, Y. V., André, M., Vaivads, A., Chasapis, A., Matthaeus, W. H., et al. (2021). Non-Maxwellianity of electron distributions near Earth's magnetopause. *Journal of Geophysical Research: Space Physics*, *126*(10), e2021JA029260. https://doi.org/10.1029/2021ja029260

Gunell, H., Stenberg Wieser, G., Mella, M., Maggiolo, R., Nilsson, H., Darrouzet, F., et al. (2014). Waves in high-speed plasmoids in the magnetosheath and at the magnetopause. In *Annales Geophysicae* (Vol. *32*, pp. 991–1009).

Hietala, H., Laitinen, T. V., Andréeová, K., Vainio, R., Vaivads, A., Palmroth, M., et al. (2009). Supermagnetosonic jets behind a collisionless quasiparallel shock. *Physical Review Letters*, *103*(24), 245001. https://doi.org/10.1103/physrevlett.103.245001

Hietala, H., Partamies, N., Laitinen, T., Clausen, L. B., Facskó, G., Vaivads, A., et al. (2012). Supermagnetosonic subsolar magnetosheath jets and their effects: From the solar wind to the ionospheric convection. In *Annales Geophysicae* (Vol. *30*, pp. 33–48).

Hietala, H., Phan, T., Angelopoulos, V., Oieroset, M., Archer, M. O., Karlsson, T., & Plaschke, F. (2018). In situ observations of a magnetosheath high-speed jet triggering magnetopause reconnection. *Geophysical Research Letters*, *45*(4), 1732–1740. https://doi.org/10.1002/2017gl076525

Hietala, H., & Plaschke, F. (2013). On the generation of magnetosheath high-speed jets by bow shock ripples. *Journal of Geophysical Research: Space Physics*, *118*(11), 7237–7245. https://doi.org/10.1002/2013ja019172

Kajdič, P., Raptis, S., Blanco-Cano, X., & Karlsson, T. (2021). Causes of jets in the quasi-perpendicular magnetosheath. *Geophysical Research Letters*, *48*(13), e2021GL093173. https://doi.org/10.1029/2021gl093173

Karlsson, T., Kullen, A., Liljeblad, E., Brenning, N., Nilsson, H., Gunell, H., & Hamrin, M. (2015). On the origin of magnetosheath plasmoids and their relation to magnetosheath jets. *Journal of Geophysical Research: Space Physics*, *120*(9), 7390–7403. https://doi.org/10.1002/2015ja021487

Karlsson, T., Plaschke, F., Hietala, H., Archer, M., Blanco-Cano, X., Kajdič, P., et al. (2018). Investigating the anatomy of magnetosheath jets–MMS observations. In *Annales Geophysicae* (Vol. *36*, pp. 655–677).

Karlsson, T., Raptis, S., Trollvik, H., & Nilsson, H. (2021). Classifying the magnetosheath behind the quasi-parallel and quasi-perpendicular bow shock by local measurements. *Journal of Geophysical Research: Space Physics*, *126*(9), e2021JA029269. https://doi.org/10.1029/2021ja029269

Katsavrias, C., Raptis, S., Daglis, I. A., Karlsson, T., Georgiou, M., & Balasis, G. (2021). On the generation of Pi2 pulsations due to plasma flow patterns around magnetosheath jets. *Geophysical Research Letters*, *48*(15), e2021GL093611. https://doi.org/10.1029/2021gl093611

King, J., & Papitashvili, N. (2005). Solar wind spatial scales in and comparisons of hourly wind and ace plasma and magnetic field data. *Journal of Geophysical Research*, *110*(A2), A02104. https://doi.org/10.1029/2004ja010649

Koller, F., Temmer, M., Preisser, L., Plaschke, F., Geyer, P., Jian, L. K., et al. (2022). Magnetosheath jet occurrence rate in relation to CMEs and SIRs. *Journal of Geophysical Research: Space Physics*, *127*(4), e2021JA030124. https://doi.org/10.1029/2021ja030124

LaMoury, A. T., Hietala, H., Plaschke, F., Vuorinen, L., & Eastwood, J. P. (2021). Solar wind control of magnetosheath jet formation and propagation to the magnetopause. *Journal of Geophysical Research: Space Physics*, *126*(9), e2021JA029592. https://doi.org/10.1029/2021ja029592

Li, H., Jiang, W., Wang, C., Verscharen, D., Zeng, C., Russell, C., et al. (2020). Evolution of the Earth's magnetosheath turbulence: A statistical study based on MMS observations. *The Astrophysical Journal Letters*, *898*(2), L43. https://doi.org/10.3847/2041-8213/aba531

Li, Y.-X., Li, W.-Y., Tang, B.-B., Norgren, C., He, J.-S., Wang, C., et al. (2021). Quantification of cold-ion beams in a magnetic reconnection jet. *Frontiers in Astronomy and Space Sciences*, *8*, 745264. https://doi.org/10.3389/fspas.2021.745264

Liu, T. Z., Angelopoulos, V., Hietala, H., & Wilson, L. B., III (2017). Statistical study of particle acceleration in the core of foreshock transients. *Journal of Geophysical Research: Space Physics*, *122*(7), 7197–7208. https://doi.org/10.1002/2017ja024043

Liu, T. Z., Hietala, H., Angelopoulos, V., Omelchenko, Y., Roytershteyn, V., & Vainio, R. (2019). THEMIS observations of particle acceleration by a magnetosheath jet-driven bow wave. *Geophysical Research Letters*, *46*(14), 7929–7936. https://doi.org/10.1029/2019gl082614

Liu, T. Z., Hietala, H., Angelopoulos, V., Vainio, R., & Omelchenko, Y. (2020). Electron acceleration by magnetosheath jet-driven bow waves. *Journal of Geophysical Research: Space Physics*, *125*(7), e2019JA027709. https://doi.org/10.1029/2019ja027709

Liu, T. Z., Zhang, H., Turner, D., Vu, A., & Angelopoulos, V. (2022). Statistical study of favorable foreshock ion properties for the formation of hot flow anomalies and foreshock bubbles. *Journal of Geophysical Research: Space Physics*, *127*(8), e2022JA030273. https://doi.org/10.1029/2022ja030273

Lucek, E., Constantinescu, D., Goldstein, M., Pickett, J., Pincon, J.-L., Sahraoui, F., et al. (2005). The magnetosheath. *Space Science Reviews*, *118*(1), 95–152. https://doi.org/10.1007/s11214-005-3825-2

Ng, J., Chen, L.-J., & Omelchenko, Y. (2021). Bursty magnetic reconnection at the Earth's magnetopause triggered by high-speed jets. *Physics of Plasmas*, *28*(9), 092902. https://doi.org/10.1063/5.0054394

Norenius, L., Hamrin, M., Goncharov, O., Gunell, H., Opgenoorth, H., Pitkänen, T., et al. (2021). Ground-based magnetometer response to impacting magnetosheath jets. *Journal of Geophysical Research: Space Physics*, *126*(8), e2021JA029115. https://doi.org/10.1029/2021ja029115

Omelchenko, Y., Chen, L.-J., & Ng, J. (2021). 3D space-time adaptive hybrid simulations of magnetosheath high-speed jets. *Journal of Geophysical Research: Space Physics*, *126*(7), e2020JA029035. https://doi.org/10.1029/2020ja029035

Palmroth, M., Raptis, S., Suni, J., Karlsson, T., Turc, L., Johlander, A., et al. (2021). Magnetosheath jet evolution as a function of lifetime: Global hybrid-Vlasov simulations compared to MMS observations. In *Annales Geophysicae* (Vol. *39*, pp. 289–308).

Paschmann, G., & Daly, P. W. (1998). Analysis methods for multi-spacecraft data. ISSI scientific reports series SR-001, ESA/ISSI, Vol. 1. ISBN 1608-280X, 1998. *ISSI Scientific Reports Series*, *1*.

Perri, S., Perrone, D., Yordanova, E., Sorriso-Valvo, L., Paterson, W., Gershman, D., et al. (2020). On the deviation from Maxwellian of the ion velocity distribution functions in the turbulent magnetosheath. *Journal of Plasma Physics*, *86*(1), 905860108. https://doi.org/10.1017/s0022377820000021

Plaschke, F., Hietala, H., & Angelopoulos, V. (2013). Anti-sunward high-speed jets in the subsolar magnetosheath. In *Annales Geophysicae* (Vol. *31*, pp. 1877–1889).

Plaschke, F., Hietala, H., Archer, M., Blanco-Cano, X., Kajdič, P., Karlsson, T., et al. (2018). Jets downstream of collisionless shocks. *Space Science Reviews*, *214*(5), 1–77. https://doi.org/10.1007/s11214-018-0516-3

Plaschke, F., Jernej, M., Hietala, H., & Vuorinen, L. (2020). On the alignment of velocity and magnetic fields within magnetosheath jets. In *Annales Geophysicae* (Vol. *38*, pp. 287–296).

Plaschke, F., Karlsson, T., Hietala, H., Archer, M., Vörös, Z., Nakamura, R., et al. (2017). Magnetosheath high-speed jets: Internal structure and interaction with ambient plasma. *Journal of Geophysical Research: Space Physics*, *122*(10), 10–157. https://doi.org/10.1002/2017ja024471

Pollock, C., Moore, T., Jacques, A., Burch, J., Gliese, U., Saito, Y., et al. (2016). Fast plasma investigation for magnetospheric multiscale. *Space Science Reviews*, *199*(1), 331–406.

Preisser, L., Blanco-Cano, X., Kajdič, P., Burgess, D., & Trotta, D. (2020). Magnetosheath jets and plasmoids: Characteristics and formation mechanisms from hybrid simulations. *The Astrophysical Journal Letters*, *900*(1), L6. https://doi.org/10.3847/2041-8213/abad2b

Raptis, S. (2022). *SavvasRaptis/Jets-VDFS: Revised release*. Zenodo. https://doi.org/10.5281/zenodo.7215235

Raptis, S., Aminalragia-Giamini, S., Karlsson, T., & Lindberg, M. (2020). Classification of magnetosheath jets using neural networks and High Resolution OMNI (HRO) Data. *Frontiers in Astronomy and Space Sciences*, *7*, 24. https://doi.org/10.3389/fspas.2020.00024

Raptis, S., Karlsson, T., Plaschke, F., Kullen, A., & Lindqvist, P.-A. (2020). Classifying magnetosheath jets using MMS: Statistical properties. *Journal of Geophysical Research: Space Physics*, *125*(11), e2019JA027754. https://doi.org/10.1029/2019ja027754

Raptis, S., Karlsson, T., Vaivads, A., Pollock, C., Plaschke, F., Johlander, A., et al. (2022). Downstream high-speed plasma jet generation as a direct consequence of shock reformation. *Nature Communications*, *13*(1), 598. https://doi.org/10.1038/s41467-022-28110-4

Russell, C., Anderson, B., Baumjohann, W., Bromund, K., Dearborn, D., Fischer, D., et al. (2016). The magnetospheric multiscale magnetometers. *Space Science Reviews*, *199*(1), 189–256. https://doi.org/10.1007/s11214-014-0057-3

Safrankova, J., Nemecek, Z., & Santolik, O. (1994). Ion distribution function in the magnetosheath: Fine structure. *Advances in Space Research*, *14*(7), 31–34. https://doi.org/10.1016/0273-1177(94)90044-2

Shue, J.-H., Song, P., Russell, C. T., Steinberg, J. T., Chao, J. K., Zastenker, G., et al. (1998). Magnetopause location under extreme solar wind conditions. *Journal of Geophysical Research*, *103*(A8), 17691–17700. https://doi.org/10.1029/98JA01103

Sibeck, D., Lee, S.-H., Omidi, N., & Angelopoulos, V. (2021). Foreshock cavities: Direct transmission through the bow shock. *Journal of Geophysical Research: Space Physics*, *126*(5), e2021JA029201. https://doi.org/10.1029/2021ja029201

Suni, J., Palmroth, M., Turc, L., Battarbee, M., Johlander, A., Tarvus, V., et al. (2021). Connection between foreshock structures and the generation of magnetosheath jets: Vlasiator results. *Geophysical Research Letters*, *48*(20), e2021GL095655. https://doi.org/10.1029/2021gl095655

Tinoco-Arenas, A., Kajdič, P., Preisser, L., Blanco-Cano, X., Trotta, D., & Burgess, D. (2022). Parametric study of magnetosheath jets in 2D local hybrid simulations. *Frontiers in Astronomy and Space Sciences*, *9*, 793195. https://doi.org/10.3389/fspas.2022.793195

Vogt, J., Haaland, S., & Paschmann, G. (2011). Accuracy of multi-point boundary crossing time analysis. In *Annales Geophysicae* (Vol. *29*, pp. 2239–2252).

Vörös, Z., Yordanova, E., Graham, D. B., Khotyaintsev, Y. V., & Narita, Y. (2019). MMS observations of whistler and lower hybrid drift waves associated with magnetic reconnection in the turbulent magnetosheath. *Journal of Geophysical Research: Space Physics*, *124*(11), 8551–8563. https://doi.org/10.1029/2019ja027028

Vuorinen, L., Hietala, H., & Plaschke, F. (2019). Jets in the magnetosheath: IMF control of where they occur. In *Annales Geophysicae* (Vol. *37*, pp. 689–697).

Vuorinen, L., Hietala, H., Plaschke, F., & LaMoury, A. T. (2021). Magnetic field in magnetosheath jets: A statistical study of B_z near the magnetopause. *Journal of Geophysical Research: Space Physics*, *126*(9), e2021JA029188. https://doi.org/10.1029/2021ja029188

Vuorinen, L., Vainio, R., Hietala, H., & Liu, T. Z. (2022). Monte Carlo simulations of electron acceleration at bow waves driven by fast jets in the Earth's magnetosheath. *The Astrophysical Journal*, *934*(2), 165. https://doi.org/10.3847/1538-4357/ac7f42

Wang, B., Nishimura, Y., Hietala, H., Lyons, L., Angelopoulos, V., Plaschke, F., et al. (2018). Impacts of magnetosheath high-speed jets on the magnetosphere and ionosphere measured by optical imaging and satellite observations. *Journal of Geophysical Research: Space Physics*, *123*(6), 4879–4894. https://doi.org/10.1029/2017ja024954

Wilson, L. (2016). Low frequency waves at and upstream of collisionless shocks. *Washington DC American Geophysical Union Geophysical Monograph Series*, *216*, 269–291. https://doi.org/10.1002/9781119055006.ch16

Yordanova, E., Vörös, Z., Raptis, S., & Karlsson, T. (2020). Current sheet statistics in the magnetosheath. *Frontiers in Astronomy and Space Sciences*, *7*, 2. https://doi.org/10.3389/fspas.2020.00002